

**Planetary boundary
influence at the
Jungfrauoch**

M. Collaud Coen et al.

This discussion paper is/has been under review for the journal Atmospheric Chemistry and Physics (ACP). Please refer to the corresponding final paper in ACP if available.

Planetary boundary influence at the Jungfrauoch analyzed by aerosol cycles and synoptic weather types

M. Collaud Coen¹, E. Weingartner², M. Furger², S. Nyeki³, A. S. H. Prévôt², M. Steinbacher⁴, and U. Baltensperger²

¹MeteoSwiss, Aerological Station, Les Invuardes, 1530 Payerne, Switzerland

²Laboratory of Atmospheric Chemistry, Paul Scherrer Institut, 5232 Villigen PSI, Switzerland

³Physikalisch-Meteorologisches Observatorium Davos and Word Radiation Center (PMOD/WRC), 7260 Davos Dorf, Switzerland

⁴Empa, Swiss Federal Laboratories for Materials Science and Technology, 8600 Dübendorf, Switzerland

Received: 3 December 2010 – Accepted: 13 December 2010 – Published: 14 January 2011

Correspondence to: M. Collaud Coen (martine.collaud@meteoswiss.ch)

Published by Copernicus Publications on behalf of the European Geosciences Union.

Title Page	
Abstract	Introduction
Conclusions	References
Tables	Figures
◀	▶
◀	▶
Back	Close
Full Screen / Esc	
Printer-friendly Version	
Interactive Discussion	



Abstract

Fourteen years of meteorological parameters, aerosol variables (absorption and scattering coefficients, aerosol number concentration) and trace gases (CO, NO_x, SO₂) measured at the Jungfraujoch (JFJ, 3580 m a.s.l.) have been analyzed as a function of different synoptic weather types. The Alpine Weather Statistics (AWS) classification was used to define the synoptic meteorology over the whole Swiss region. The seasonal contribution of each synoptic weather type to the aerosol concentration was deduced from the aerosol annual cycles while the planetary boundary layer (PBL) influence was estimated by means of the diurnal cycles. Since aerosols are scavenged by precipitation, the diurnal cycle of the CO concentration was also used to identify polluted air masses. SO₂ and NO_x concentrations were used as precursor tracers for new particle formation and growth. This study confirms the consensus view that the JFJ is mainly influenced by the free troposphere during winter and by injection of air parcels from the PBL during summer. A more detailed picture is, however, drawn where the JFJ is completely influenced by free tropospheric air masses in winter during advective weather types and largely influenced by the PBL also during the night in summer during the subsidence weather type. Between these two extreme situations, the PBL influence at the JFJ depends on both the time of year and the synoptic weather type. The fraction of PBL air transported to the JFJ was estimated by the relative increase of the specific humidity and CO.

1 Introduction

The Jungfraujoch (JFJ) Sphinx research station is situated at 3580 m a.s.l. in the middle of the Swiss Alps. Since 1995 continuous aerosol and trace gas measurements have been performed at this site within the Global Atmosphere Watch (GAW) program of the World Meteorological Organization. Due to its high elevation, the JFJ research station allows investigation of the lower free troposphere (FT) over Central Europe and

ACPD

11, 985–1024, 2011

Planetary boundary influence at the Jungfraujoch

M. Collaud Coen et al.

Title Page

Abstract

Introduction

Conclusions

References

Tables

Figures

◀

▶

◀

▶

Back

Close

Full Screen / Esc

Printer-friendly Version

Interactive Discussion



Planetary boundary influence at the Jungfraujoch

M. Collaud Coen et al.

Title Page

Abstract

Introduction

Conclusions

References

Tables

Figures

⏪

⏩

◀

▶

Back

Close

Full Screen / Esc

Printer-friendly Version

Interactive Discussion



the mixing of planetary boundary layer (PBL) and FT air masses. It is recognized as a station measuring FT air masses, even if the JFJ is partially influenced by the PBL. Saharan dust events lasting from several hours to 2 days occur mostly during the spring and in October to November (Collaud Coen et al., 2004). The annual cycle of all measured aerosol variables (absorption coefficient b_{abs} and scattering coefficients b_{scat} , aerosol number concentration N , aerosol surface area concentration, chemical composition, particle mass concentration, radon decay product concentration), which attain a maximum in summer and a minimum in winter, can be attributed to the vertical transport of PBL air masses by thermally-driven convection occurring from late spring to late summer (Baltensperger et al., 1997; Lugauer et al., 1998, 2000). Autumn is far less influenced by this dominant transport mode (Lugauer et al., 1998, 2000). The regional extent of thermally-driven convection was studied during an airborne lidar campaign over the JFJ and the Swiss Alps. The gradual evolution of the PBL on a summer day in 1997 clearly showed that the PBL attained a near-uniform height of up to 4200 m a.s.l. by the early afternoon (Nyeki et al., 2000). A later in-situ and airborne study by Henne et al. (2004) reported that PBL air was efficiently injected into the altitude range from 2000 to 4000 m a.s.l. where it had a substantial influence on air mass chemistry (Henne et al., 2005a). These processes are important from May to September, especially in summer (Henne et al., 2005b), so that the transport mechanisms of air masses to the JFJ during the warmest months depend mainly on these PBL injections over the whole Alpine area rather than on the local, thermally induced upslope wind. This annual cycle was observed in long-term measurements of several in-situ aerosol variables (b_{abs} , b_{scat} , N , etc.) (Nyeki et al., 1998a). Long-term trends were found to be positive and statistically significant in winter, when the FT influence at the JFJ is the greatest (Collaud Coen et al., 2007). The PBL influence does not modify the aerosol size distribution to any large extent, but mainly influences the concentration of accumulation mode particles (Weingartner et al., 1999; Nyeki et al., 1998b). Kammermann et al. (2010) found that the submicrometer sized particles exhibit a slightly lower hygroscopicity during PBL influence which is explained by a relatively larger fraction of

less hygroscopic compounds such as organic matter compared to more hygroscopic inorganic salts. However, this effect of PBL influence is not seen in a seasonality of the hygroscopicity because the effect is small. Diurnal cycles are observed for all the measured aerosol variables during the warm months and are more pronounced in convective meteorological situations (Weingartner et al., 1999; Lugauer et al., 2000). Analyses of the aerosol surface area concentration, concentrations of radon decay products, and the total aerosol mass concentration as a function of the Alpine Weather Statistics (AWS) scheme show that synoptic-scale lifting processes occur occasionally in winter and more significantly in April. In addition, maximum values in aerosol variables are attained during anticyclonic conditions (Lugauer et al., 1998, 2000). It was also shown that transport of gaseous and aerosol species is similar during anticyclonic but different during cyclonic conditions.

In this paper, the influence of the PBL at the JFJ is refined by analyzing the 14-year data set (1995–2008) of mean annual and diurnal cycles as a function of synoptic weather type defined by Schüepp (1979) in the AWS. This parameterization of synoptic weather type allows the synoptic meteorology to be described over the whole Swiss region. Meteorological parameters measured at JFJ further characterize local meteorological conditions at the aerosol measurement site. Aerosols are one of the most sensitive parameters to the influence of the PBL (due to a strong vertical gradient), so that the analysis of N , b_{abs} , b_{scat} and the scattering Ångström exponent (\hat{a}_{scat}) allows information on the transport of air masses from the PBL to the JFJ to be gained. N is the most sensitive to the formation of new particles, and the absorption coefficient is most sensitive to polluted air masses. However, as aerosols in contrast to most gaseous species are removed by precipitation, CO measurements are useful in characterizing the PBL influence during precipitation. In addition, the relative increase of CO and the specific humidity (remains constant during vertical motion in the absence of precipitation) will allow the export of PBL air to the JFJ to be quantified. Finally, SO_2 and NO_x will be used as tracers for aerosol number and mass precursors.

**Planetary boundary
influence at the
Jungfraujoch**

M. Collaud Coen et al.

Title Page

Abstract

Introduction

Conclusions

References

Tables

Figures

◀

▶

◀

▶

Back

Close

Full Screen / Esc

Printer-friendly Version

Interactive Discussion



2 Experiment

2.1 Measurement site

The JFJ high alpine research station (46°33' N, 7°59' E) is located on a mountain crest on the northern edge of the Swiss Alps. The saddle position of the JFJ, between the Jungfrau (4158 m a.s.l.) and the Mönch (4089 m a.s.l.) mountains, channels the local horizontal flow in a north-western or south-eastern direction. With north-westerly wind directions, air-masses from over the Swiss plateau are advected to the JFJ, while during south-easterly wind direction, air-masses come from the inner alpine area and from South of the Alps. Contamination due to local sources is rare as electricity is supplied by a high-voltage connection from the valley. A local diesel generator is only in operation for short periods during power failures. Emissions due to tourist activities are usually negligible. All diurnal times mentioned in this study are given as local standard time LST (equal to UTC+1 h).

2.2 Instrumentation and methods

Ambient aerosol particles were sampled and measured at the old JFJ research station (3454 m a.s.l.) from 1995 to January 1998 and at the JFJ Sphinx research station (3580 m a.s.l.) thereafter with a new inlet. At both sites, the aerosol is first brought into the laboratory (mean temperature of 22(±2) °C), which lowers the relative humidity (RH) to below 20%. Therefore cloud droplets are evaporated at an early stage of the sampling process, so that only dried aerosols are measured. Calculations for the latter inlet set-up showed that cloud droplets with a diameter smaller than 40 μm can be sampled at wind speeds of up to 20 m s⁻¹ (Weingartner et al., 1999). No discontinuities induced by the altitude and inlet changes were detected in the aerosol data sets (Collaud Coen et al., 2007).

The aerosol light scattering and backscattering coefficients were measured at three wavelengths ($\lambda=450, 550$ and 700 nm) by an integrating nephelometer (IN, TSI 3563)

Planetary boundary influence at the Jungfraujoch

M. Collaud Coen et al.

Title Page

Abstract

Introduction

Conclusions

References

Tables

Figures



Back

Close

Full Screen / Esc

Printer-friendly Version

Interactive Discussion



and were corrected for the truncation error according to Anderson and Ogren (1998) and Nessler et al. (2005), which makes use of the scattering Ångström exponent \hat{a}_{scat} to calculate the wavelength dependent correction factor. The value of \hat{a}_{scat} was obtained by fitting b_{scat} with a power-law dependence $b_{\text{scat}} = \beta_{\text{scat}} \cdot \lambda^{\hat{a}_{\text{scat}}}$.

The aerosol light absorption coefficients were measured by two different aethalometers. A “white light” aethalometer (AE-10, Magee Scientific) with a broad spectral range from 500 nm to 1100 nm and a peak sensitivity in the near IR at about 840 nm (Weingartner et al., 2003) was used until March 2001. A 7-wavelength aethalometer (AE-31, Magee Scientific) with narrow band light sources in the wavelength range 370–950 nm was operated thereafter. The absorption coefficients for both aethalometers were calculated by the correction method described by Collaud Coen et al. (2010). The multiple scattering constant $C_{\text{ref}} = 2.88$ was determined by comparing the absorption coefficients from a multi-angle absorption photometer and the multi-wavelength aethalometer and was applied to the AE-31. A slightly higher value for the AE-10, $C_{\text{ref}} = 2.97$, was estimated by normalizing both datasets, and is anticipated since the AE-10 filter tapes differ from those of the AE-31. For analysis of the whole 1995–2008 period, the $\lambda = 880$ nm channel from the AE-31 was chosen as it is closest to the maximum light source intensity of the AE-10.

The aerosol number concentration was measured using a TSI 3025 condensation particle counter (CPC) before March 1997, and a TSI 3010 thereafter. Although both CPCs have slightly different lower aerosol diameter cut-offs, all data were considered since only the cycles and not the trends were studied in this paper.

All meteorological parameters, (temperature T , relative humidity RH, global short wave radiation W (from $\lambda = 200$ nm to $\lambda = 3.6$ μm), erythemally weighted ultra-violet radiation UV (from $\lambda = 200$ nm to $\lambda = 340$ nm), and wind speed and direction) were measured by MeteoSwiss at the JFJ and Payerne (46.82° N, 6.95° E, 491 m a.s.l.) Swiss-MetNet stations. Precipitation is not measured at the JFJ, but daily precipitation (from 05:40 a.m. to 5:40 a.m. the day after) is measured at the Kleine Scheidegg (2061 m a.s.l.) located at the foot of the Eiger mountain next to the Mönch and the JFJ.

Planetary boundary influence at the Jungfraujoch

M. Collaud Coen et al.

Title Page

Abstract

Introduction

Conclusions

References

Tables

Figures

◀

▶

◀

▶

Back

Close

Full Screen / Esc

Printer-friendly Version

Interactive Discussion



**Planetary boundary
influence at the
Jungfraujoch**

M. Collaud Coen et al.

Title Page

Abstract

Introduction

Conclusions

References

Tables

Figures

◀

▶

◀

▶

Back

Close

Full Screen / Esc

Printer-friendly Version

Interactive Discussion



Continuous trace gas measurements are performed at the JFJ Sphinx laboratory as part of the Swiss National Air Pollution Monitoring Network (NABEL). CO is measured with cross flow modulated non-dispersive infrared absorption technology (NDIR, Horiba APMA-360; since June 2007, APMA-370). NO and NO_x are determined with chemiluminescence detectors (Ecophysics CLD 770 AL ppt, and CLD89p since January 2007). NO_x is analyzed as NO after photolytic conversion (Ecophysics PLC 760, and Ecophysics PLC 762 since 2000). SO₂ was previously measured as 24-h bulk samples by wet chemical absorption of SO₂ in a hydrogen peroxide solution and subsequent off-line analysis with ion chromatography. Since January 2007, SO₂ has been measured on-line with a UV fluorescence instrument (Thermo Electro Cooperation, Enviromental Instruments, TEI43C TL). The trace gas observations at Payerne used in this study (CO with a Horiba APMA-360; SO₂ with a MonitorLabs 8850S, since June 2000, TEI43C TL) are also conducted within the NABEL network. All gaseous concentrations are given in ppbv.

Median values were calculated for the aerosol and gas-phase variables that are neither normally nor lognormally distributed, while for normally distributed variables arithmetic mean values were computed. Confidence limits of the medians were calculated by a nonparametric method defined by an order statistic (i.e., rank observation) and using the cumulative binomial distribution (Gibbons and Coleman, 2001). A running 30-day average was also applied to the annual cycles. For the annual cycles of aerosol variables, the contributions of each synoptic weather type to the averaged annual cycles were determined by weighting the measured variables during the defined weather type by its frequency of occurrence.

2.3 Alpine weather statistics scheme

The Alpine Weather Statistics (AWS) scheme (Schüepp, 1979; SMI, 1985) is a synoptic weather type classification system based on the diurnal analysis of the pressure distribution at the surface and at 500 hPa (~5.6 km a.s.l.). It is defined for a circular area (radius of 222 km) centered 80 km east of the JFJ (46°30' N, 9° E) and covering

Switzerland and western Austria. The classification into 40 weather situations is determined by the combination of four key parameters (Schüepp, 1979; Wanner et al., 1998):

1. speed of the surface wind derived from the surface pressure gradient,
2. direction and speed of the 500 hPa wind,
3. height of the 500 hPa surface over the central point of the system,
4. baroclinicity.

These 40 weather situations can be grouped into three basic (convective, advective and mixed) and eight extended weather types (Table 1).

The convective types describe weather situations where the vertical motion predominantly influences the weather, either as a single effect or in connection with the effects of horizontal motion. The three convective weather types differ by the sign of the synoptic scale vertical motion (Lugauer et al., 1998). Divergence at low altitude caused by subsidence is predominant for the anticyclonic type CA, resulting in adiabatic warming and cloud dissipation. Ascent of air caused by convergence at low altitude is predominant for the cyclonic type CC, resulting in adiabatic cooling and cloud formation with subsequent precipitation. The convective indifferent weather type CI is characterized by a flat pressure distribution and therefore alternating small-scale up- and downdrafts depending on the effects of the terrain (Schüepp and Schirmer, 1977). The difference in the synoptic scale vertical motion of weather types CA and CC results in differences in the thermodynamic variables that are considerably more pronounced than between the four advective weather types.

The advective types include weather situations where the horizontal motion of the atmosphere is predominant, so that in flat terrain the vertical wind components are unimportant. However, the orography of the Alps adds vertical components to this air flow resulting in well-marked upslope and lee phenomena (Schüepp and Schirmer, 1977; Henne et al., 2004) such as Foehn. Eight wind sectors of 45° are distinguished

Planetary boundary influence at the Jungfraujoch

M. Collaud Coen et al.

Title Page

Abstract

Introduction

Conclusions

References

Tables

Figures



Back

Close

Full Screen / Esc

Printer-friendly Version

Interactive Discussion



**Planetary boundary
influence at the
Jungfraujoch**

M. Collaud Coen et al.

Title Page

Abstract

Introduction

Conclusions

References

Tables

Figures

⏪

⏩

◀

▶

Back

Close

Full Screen / Esc

Printer-friendly Version

Interactive Discussion



depending on the wind direction at the 500 hPa level over the central alpine area. The number of sectors within each advective type is different (Table 1). The AW type comprises only one wind sector and is characterized by advection of maritime air masses from the Atlantic. The AN type comprises two wind sectors and occurs when the Alps are influenced by cold polar air masses after a cyclone has passed to the north of Switzerland (Schüepp, 1979). The AE type comprises three wind sectors and represents situations when the usual zonal circulation is blocked. The AS type comprises two wind sectors and induces most precipitation on the southern side of the Alps. Vertical motion due to the alpine orography during advective types is often associated with cloud formation and precipitation on the upwind side. The aerosol concentration at high alpine sites is therefore not only determined by the different origin of air masses but also by modifications arising from the forced vertical motion. This is reflected in the small differences in aerosol concentration for each advective type associated with high differences in aerosol concentration between the JFJ and Colle Gnifetti (4452 m a.s.l., approximately 75 km southwest of the JFJ) (Lugauer et al., 1998).

The mixed type M describes weather situations where both the horizontal and the vertical wind components are significant, and occurs when an active cyclone or a front is present in the surface chart.

The weather types AW, AN, and AE show similar annual and diurnal cycles for aerosol and some meteorological parameters and hence these three types were grouped (AW+N+E) in the analyses and the figures for clarity.

3 Results

3.1 Occurrence and annual cycle of AWS weather types

The mean frequency distribution of AWS weather types during the 1995–2008 period is presented in Fig. 1 for each month. Advective weather types are seen to predominate during winter and convective weather types during the rest of the year. Similar

annual frequency distributions were calculated by Wanner for the 1945–1994 period (Wanner et al., 1998; Stefanicki et al., 1998) and by Lugauer for the 1988–1996 period (Lugauer et al., 1998). The mixed weather type frequency is fairly constant during the year, always ranging between 5% and 8%. Within the convective weather types, CI predominates almost during the whole year with a clear annual cycle that reaches a maximum in summer (~40%) and a minimum in winter (~20%). The CA type also occurs often (10–35%), however, without a very clear annual cycle. The CC type occurs more frequently during spring and autumn, but its frequency never exceeds 11%. Advective weather types have an inverse annual cycle to the CI type, with a minimum occurrence during summer (~20%) and a maximum occurrence during winter (45–50%) when vertical motion is suppressed by enhanced stability of the atmosphere (Schüepp and Schirmer, 1977). All the extended advective weather types show similar annual cycles with AN being the most frequent wind sector and AE the least frequent.

Schwarb (1996), as well as Stefanicki et al. (1998) and Wanner et al. (1998) showed that there has been an increase in frequency of convective weather situations and a concurrent decrease in frequency of advective weather situations since the early 1970s. These are strongly correlated with the North Atlantic Oscillation (NAO) index and are due to higher surface air pressure and lower horizontal pressure gradients. Table 2 gives the frequency distribution of AWS weather types for the 1945–1994 (Wanner et al., 1998), the 1988–1996 (Lugauer et al., 1998) and the 1995–2008 periods. The two more recent periods clearly have a greater occurrence of CA and CI weather type, a slightly lower occurrence of lifting CC and a substantially lower frequency of all advective weather types than the former period. The mixed weather type M occurred 6% of the time for both the 1945–1994 and the 1995–2008 periods, whereas the occurrence is lower for the 1988–1996 period.

3.2 Mean annual and diurnal cycles of meteorological parameters

The mean 14-year annual cycles of T , RH, W at the JFJ and precipitation (at the Kleine Scheidegg) are presented in Fig. 2 and the corresponding mean diurnal cycles for the

Planetary boundary influence at the Jungfraujoch

M. Collaud Coen et al.

Title Page

Abstract

Introduction

Conclusions

References

Tables

Figures



Back

Close

Full Screen / Esc

Printer-friendly Version

Interactive Discussion



April-May period in Fig. 3. The UV cycles are similar to the W cycles and will therefore not be presented here. Diurnal cycles of precipitation are not shown either since only daily values are available at the Kleine Scheidegg. As explained in Sect. 3.3, the year has been divided into 5 periods according to different aerosol characteristics rather than meteorological seasons.

During the CA weather type associated with subsidence, T , W and UV are higher and the RH and the precipitation lower than for all other weather types during the whole year. Contrary to all other weather types, the RH annual cycle is well defined during CA situations, with a minimum in January (45%) and a broad maximum in the May–August period. All these features can be explained by the adiabatic warming and cloud dissipation induced by CA situations. CA situations also generally present the largest T , W and RH diurnal cycles (Fig. 3, Table 3).

During the CC weather type associated with lifting, T is lower than for all other weather types. A marked minimum in T is found in February–March and can be explained by a greater occurrence of CC with northerly upper wind (52%) than during the rest of the year (30%), leading to a large influence of arctic air masses. A climatology of the Swiss Alps (Urfer, 1979) describes February as the coldest month for regions higher than 1500 m a.s.l. as well as the month with a large number of extreme cases leading to a minimum in T far lower than the mean T for the whole northern region of the Alps. During the whole year, CC situations are also characterized by high RH and precipitation and intermediate W and UV values.

The CI weather type leads to T and RH values between those of CA and CC, but to lower cloud coverage than for CC (as seen by W) and to more precipitation than for CA.

The advective weather types from W, N and E lead to rather low T during the whole year, associated with a small diurnal cycle in T ; RH shows a continuous decrease during the day that is superimposed on a diurnal cycle similar to that of aerosols. The advective type W is associated with a high amount of precipitation, and type E with very low precipitation (not shown).

Planetary boundary influence at the Jungfraujoch

M. Collaud Coen et al.

Title Page

Abstract

Introduction

Conclusions

References

Tables

Figures



Back

Close

Full Screen / Esc

Printer-friendly Version

Interactive Discussion



The AS weather type exhibits higher T , RH and precipitation, and lower W than other advective situations during the whole year. It also leads to cloud coverage and a diurnal increase in RH associated with a continuous decrease in T during the day that is superimposed onto a diurnal cycle in T similar to that of aerosols (Fig. 3 and Table 3). The AS weather type usually leads to precipitation at the end of the day or the day after where the mean amount of precipitation the day after AS situations (0.23 mm) is greater than after all other weather situations (from 0.02 to 0.15 mm).

The M weather type has low W and intermediate T and RH values during the whole year (Fig. 2), and middle to high precipitation.

3.3 Median annual cycle of aerosol variables

The 1995–2008 median annual cycles of dry b_{abs} , b_{scat} and N are shown in Fig. 4a, the relative contributions of the different synoptic weather types are shown in colors; they are computed as described above in Sect. 2.2. Similar graphs with the relative contribution of each AWS weather type to the total value of each aerosol variable are provided in Fig. 4b. Note that these numbers are influenced by both the absolute values of the aerosol variables and the frequency of occurrence of the weather type, as outlined in Sect. 2.2.

The annual cycle is similar for all three aerosol variables presented in Fig. 4, with: (i) a maximum in July-August coincident with the maximum in T , (ii) a local maximum at the summer solstice, coincident with the maximum in W , as well as a second local maximum in April-May. The latter is principally due to the increase in T and convective situations (CA and CI) leading to an increase of the aerosol concentration followed by a decrease of aerosol concentration due to wet removal by increased precipitation at the end of May and the beginning of June (Figs. 1 and 2). The summer and particularly the end of July is dominated by the influence of CA (subsidence) and CI situations, which together cause 75%, 72% and 66% of b_{scat} , b_{abs} , and N , respectively. It has to be noted that increases in b_{abs} and b_{scat} in April and decreases in August are very rapid during CA situations (Fig. 4b). The smoother changes in b_{abs} and b_{scat} in April

Planetary boundary influence at the Jungfraujoch

M. Collaud Coen et al.

[Title Page](#)[Abstract](#)[Introduction](#)[Conclusions](#)[References](#)[Tables](#)[Figures](#)[◀](#)[▶](#)[◀](#)[▶](#)[Back](#)[Close](#)[Full Screen / Esc](#)[Printer-friendly Version](#)[Interactive Discussion](#)

and August during CI situations might indicate that, due to the absence of large scale subsidence, thermally driven convection is more frequent than during CA situations. The CC type (lifting) has its greatest impact on all aerosol variables during the spring, and the advective weather types are also usually at a maximum during the spring and to a lesser extent in autumn. All three aerosol variables have their minimum in winter, when the greater influence of advective types on the scattering and absorption coefficients is related to a greater frequency of occurrence of these weather types (Fig. 1).

The annual cycle of the absorption coefficient exhibits a lower local maximum in June and a higher contribution of AS in October–November than for the two other aerosol variables. The annual cycle of N (Fig. 4a) is less pronounced than those of b_{abs} and b_{scat} for all weather types, which is mainly due to the fact that N is not only influenced by vertical transport but also by new particle formation and growth, which also proceeds in winter (Weingartner et al., 1999). The annual maximum of N occurs at the summer solstice, which coincides with the maximum in W and UV intensity, enhancing new particle formation. The CC weather type makes a particularly large contribution to N in the February–April period.

However, the annual cycles of b_{abs} and particularly N are quite different if only M, AW+N+E, AS and CC weather types are considered. In this case the maxima are found in April, while the summer concentration only presents a local maximum. Each weather type thus results in a different PBL influence at the JFJ (and consequently in different aerosol properties) depending on the periods of the year. The aerosol annual cycles allow periods of the year to be defined which show significant differences. First, the November–January period is characterized by low values of the aerosol variables and by no prevalence of a particular weather type. Second, a rapid increase in aerosol variables occurs during February–March, associated with the greater influence of CC (lifting) and advective weather types. Third, CA and CI weather types are predominant during April–May. Fourth, the June–August period is characterized by maximum values in all aerosol variables, due to the largest PBL influence. Finally the September–

Planetary boundary influence at the Jungfraujoch

M. Collaud Coen et al.

Title Page

Abstract

Introduction

Conclusions

References

Tables

Figures

◀

▶

◀

▶

Back

Close

Full Screen / Esc

Printer-friendly Version

Interactive Discussion



October period is characterized by a rapid decrease in aerosol concentrations for all synoptic weather situations. These 5 periods of the year have therefore been chosen to further investigate the diurnal cycles.

3.4 Median diurnal cycles in aerosol variables

Diurnal cycles of b_{scat} , b_{abs} and N are presented in Fig. 5 for the five periods defined above. The M type is not represented in Fig. 5 since it does not correspond to a well defined meteorological situation. In addition, it occurs rarely and is never associated with high aerosol concentrations. However, its diurnal cycles are similar to those of advective situations from W, N and E most of the time.

Values of N always exhibit the most pronounced diurnal cycles, especially in winter, which are due to its greatest sensitivity to the Aitken mode aerosol, and b_{abs} exhibits the least distinct diurnal cycles in all cases. The June–August period always leads to well defined diurnal cycles of N , with large amplitudes. February–March displays the weakest diurnal cycles of the year, with b_{abs} showing no defined diurnal cycles for any weather type. The November–January period also exhibits no diurnal cycles or only weak ones. The maxima are usually found between 14:00 and 18:00, and the minima (if well defined) between 5:00 and 7:00. In summer, all weather types also present a local maximum in b_{abs} between 8:00 and 10:00, similar to NO_x (not shown) and N that may be due to local contamination by diesel exhaust from a snowcat used for tourist purposes only in summer.

For most of the year, CA (subsidence) presents the largest diurnal cycles, and in summer both the CA maxima and minima are higher than those of the other weather types. In September–October, b_{scat} has a particularly large diurnal cycle compared to b_{abs} for the CA and CI weather types.

During CC situations, a larger diurnal cycle of b_{scat} is observed during November–March periods with the highest daily maxima, whereas the N diurnal cycle presents the same features only in February–March with high maxima and minima.

Planetary boundary influence at the Jungfraujoch

M. Collaud Coen et al.

Title Page

Abstract

Introduction

Conclusions

References

Tables

Figures

◀

▶

◀

▶

Back

Close

Full Screen / Esc

Printer-friendly Version

Interactive Discussion



During April–October periods, the AS weather type presents a continuous decrease of all aerosol variables during the day, which is superimposed onto the usual diurnal cycle during summer. Such a continuous diurnal decrease is most probably due to aerosol wet removal on the alpine windward side during AS situations.

To gain information on the amplitude of the diurnal cycles, the ratio between the maximum and the minimum values of the monthly median diurnal cycle are plotted for b_{abs} , b_{scat} , and N during CA, CC and AW+N+E weather types (Fig. 6). Diurnal cycle amplitudes are neither plotted for the AS type since a continuous diurnal decrease is usually observed, nor for the CI type since their amplitudes remain rather constant between 1.4 and 2.7 throughout the year, nor for the M type that is similar to the AW+N+E type. The annual cycles of the diurnal amplitude are almost similar for the three described aerosol variables. For the CA type (subsidence), the diurnal cycles are most pronounced in the spring (April–May) and in the autumn (September–October) and lower in summer. For the CC type (lifting), the diurnal cycles are most pronounced in January–March and in July. During advective situations from W, N and E, the diurnal cycles are most pronounced in summer for b_{abs} and b_{scat} , which is not observed for N . The inset in Fig. 6b shows the CA diurnal cycle of the scattering Ångström exponent in April, which is the only month showing a clear diurnal cycle with smaller values corresponding to larger particles in the morning, and larger values corresponding to smaller particles during the afternoon. The diurnal cycle of the aerosol size between the FT aged aerosol and the PBL aerosol is therefore only observed in April for the subsidence (CA) case.

4 Discussion

Before analyzing in detail the PBL influence at the JFJ high-alpine site as a function of the different periods of the year and synoptic weather situations, some general aspects are first considered, including: (1) the sensitivity of b_{abs} and CO to pollution from the Swiss plateau, (2) nucleation and particle growth, (3) thermal injection during CA weather types, and (4) the influence of the PBL during advective weather types.

Planetary boundary influence at the Jungfraujoch

M. Collaud Coen et al.

Title Page

Abstract

Introduction

Conclusions

References

Tables

Figures

◀

▶

◀

▶

Back

Close

Full Screen / Esc

Printer-friendly Version

Interactive Discussion



Planetary boundary influence at the Jungfraujoch

M. Collaud Coen et al.

Title Page

Abstract

Introduction

Conclusions

References

Tables

Figures

◀

▶

◀

▶

Back

Close

Full Screen / Esc

Printer-friendly Version

Interactive Discussion

1. The absorption coefficient is mostly determined by the black carbon concentration arising from combustion processes, and is hence more characteristic of polluted air masses. In contrast to aerosol particles, CO is not washed out by precipitation and can therefore also be a tracer for polluted air masses during weather situations with precipitation. However, CO diurnal cycles are less pronounced than those of other chemical species due to a longer atmospheric lifetime and thus higher background concentrations resulting in a less pronounced vertical concentration profile (Zellweger et al., 2000). In contrast, N is governed by the Aitken mode aerosol so that its diurnal and annual cycles are greatly influenced by the growth of newly formed particles. The scattering coefficient is sensitive to both primary pollution and condensational growth of the particles and thus combines characteristics of both b_{abs} and N .
2. The formation rate of new particles from gaseous precursors and their subsequent growth are enhanced by solar radiation, by lower temperature (due to higher supersaturations of the condensable gas phase species at colder temperatures; Clausius-Clapeyron equation), by high precursor concentrations and a low aerosol surface area concentration available as a condensational sink (i.e., a low concentration of accumulation mode particles). Clouds inhibit new particle formation and growth processes and enhance loss processes of newly formed particles by scavenging (Boulon et al., 2010).
3. The CA weather type is characterized by subsidence and does not induce upward vertical transport of PBL air masses on a large scale; however, the temperature and the global radiation (low cloud coverage) are a maximum during subsidence, leading to PBL growth and thermally induced injections of PBL air that can reach the altitude of the JFJ.
4. The diurnal cycles are partly used in this study to determine the PBL influence at the JFJ. Synoptic and topographic lifting during advective situations does not depend on the time of the day, so that the absence of a diurnal cycle does not

imply that there is no PBL influence. The values of aerosol variables allow the PBL influence in these cases to be estimated.

4.1 PBL influence at the JFJ

Advective weather types are predominant from November to January with a 45% frequency (Fig. 1). During this period, b_{abs} and b_{scat} are effectively dominated by the contribution of advective weather types (>40%, see Fig. 4), whereas CA and CI weather types also contribute substantially to N (50%). This difference is due to the sensitivity of N to the growth of newly-formed particles at the JFJ and in the adjacent valleys (see the diurnal cycle of N in winter, Fig. 5). The SO_2 concentration, which enhances new particle formation, is a maximum from November–April, whereas the NO_x concentration, which enhances particle growth, is a maximum in March–April and in November (Fig. 7). During winter, longer lifetimes and higher emissions (due to domestic heating, cold start engine conditions, etc.) explain the higher concentrations of primary gas phase compounds measured in the FT at the JFJ (Balzani Lööv et al., 2008). The CA and CI weather types lead to high global radiation and the lowest cloud coverage, so that their contributions to new particle formation in winter are clearly visible in the annual cycle of N (Fig. 4).

In February and March, b_{abs} , b_{scat} and N increase for all weather types, but particularly for lifting (CC) and advection from W, N and E. Lifting also shows particularly strong diurnal cycles in N and b_{scat} . The absence of a diurnal cycle in b_{abs} shows that the increase in N and b_{scat} during the afternoon is not due to aerosol from the Swiss plateau reaching the JFJ. The high CO concentration during the whole year (Fig. 8) indicates that the CC weather type allows PBL air masses to be transported to the JFJ altitude, but that aerosols are removed most of the time by wet deposition. In February and March, the concentration of aerosol number and mass precursors is at a maximum, principally due to an increase during the CC weather type, as can be seen in the SO_2 and NO_x annual cycles (Fig. 7). This high precursor concentration is associated with relatively high global radiation at the JFJ (W is higher during CC than during M

Planetary boundary influence at the Jungfraujoch

M. Collaud Coen et al.

Title Page

Abstract

Introduction

Conclusions

References

Tables

Figures

◀

▶

◀

▶

Back

Close

Full Screen / Esc

Printer-friendly Version

Interactive Discussion



and all advective weather types), low surface area concentrations and very low temperatures; all these parameters lead to high rates of new particle formation and thus to a diurnal cycle in N and b_{scat} . To model this dependence, the differences between the diurnal maximum and minimum in median N values at the JFJ are plotted (Fig. 9) as a function of $W \cdot [\text{SO}_2] / T^2$. The parameters W (global short wave solar radiation), $[\text{SO}_2]$ (SO₂ concentration in ppbv), and T (temperature in K) are measured at Payerne which is considered to be representative of the Swiss plateau region. In this simplified model, $[\text{SO}_2]$ is used as a proxy for all the precursor gases, while the square of the temperature was chosen to represent the temperature dependence of the Clausius-Clapeyron equation. Figure 9 shows that the high concentration of particles in February-March during lifting can be simply explained by meteorological parameters and the precursor concentration over the Swiss plateau region. This correlation is worse for other weather types, due to the decoupling between the Swiss plateau region and the JFJ during the coldest months or to lower wet removal leading to a higher condensation sink. The contribution of new particle formation is particularly visible in February-March due to the very low aerosol concentration during this period of the year. However, considering all synoptic situations, new particle formation at the JFJ is a maximum in late spring and early summer (Manninen et al., 2010; Boulon et al., 2010). The JFJ is further characterized by a high amount (22.3%) of ion-mediated nucleation and a high growth rate ($\sim 5 \text{ nm h}^{-1}$ for particles in the range $d = 1.3\text{--}20 \text{ nm}$, Boulon et al., 2010).

In April and May, the CA and CI weather types become dominant, presenting the major contribution to all aerosol variables. For subsidence (CA), large diurnal cycles are found for all aerosol variables and their amplitudes are a maximum in April for b_{abs} and b_{scat} , and in May for N . Larger diurnal amplitudes are found only during the lifting weather type (CC). The CO concentration also shows a clear diurnal cycle during subsidence, and April is the only month presenting a clear diurnal cycle of the scattering Ångström exponent indicating a larger aerosol size (low scattering Ångström exponent) from 2:00 to 12:00 and a smaller aerosol size (high scattering Ångström exponent) from 14:00 to 24:00 (see insert in Fig. 6). The influence of the PBL due to thermal convection

**Planetary boundary
influence at the
Jungfraujoch**

M. Collaud Coen et al.

Title Page

Abstract

Introduction

Conclusions

References

Tables

Figures

◀

▶

◀

▶

Back

Close

Full Screen / Esc

Printer-friendly Version

Interactive Discussion



thus occurs from April onward during the CA weather type, resulting in a higher concentration of aerosols from more polluted air masses during the afternoon, whereas FT conditions prevail during the night. This alternation of FT and PBL air masses leads to a maximum amplitude in diurnal cycles during the CA weather type. All other weather types exhibit a small diurnal cycle reflecting a very small and unsystematic increase of the PBL influence during the afternoon, while the AS weather type exhibits no diurnal cycle.

Aerosol variables are greatly enhanced in summer (June–August) during subsidence (CA) even if the frequency of occurrence of the CA weather type is not really higher than during the rest of the year; the higher aerosol concentration is due to higher temperatures inducing enhanced PBL air injection into the FT and not due to local thermally induced valley winds, as was also observed by Henne et al. (2005b). The diurnal minima of all aerosol variables are much higher in summer for the CA weather type than for other weather types. Higher aerosol concentrations during the night are due to the remaining influence of residual layers under these meteorological (high T) and synoptic conditions. All other weather types also present pronounced diurnal cycles of aerosol variables, RH and CO concentration which implies that PBL air masses reach the JFJ during the afternoon due to high values of T in summer, but that FT air masses prevail during the night. The high aerosol concentration during summer is lower at the beginning of June as a result of high precipitation, and lower in the second half of August due to both precipitation and lower W during CA weather types.

Finally, the September-October period is characterized by a less sharp decrease in aerosol variables than in August with values similar to the February-March period, but with a larger diurnal cycle for all weather types except for CC (lifting). During CA and CI weather types, b_{scat} and N have a larger diurnal cycle than b_{abs} due to higher global radiation and therefore enhanced new particle formation and growth. During autumn, thermally driven convection above the temperature inversion frequently brings high-alpine air masses to the JFJ (Lugauer et al., 2000).

Planetary boundary influence at the Jungfraujoch

M. Collaud Coen et al.

Title Page

Abstract

Introduction

Conclusions

References

Tables

Figures

◀

▶

◀

▶

Back

Close

Full Screen / Esc

Printer-friendly Version

Interactive Discussion



Planetary boundary influence at the Jungfraujoch

M. Collaud Coen et al.

Title Page

Abstract

Introduction

Conclusions

References

Tables

Figures

◀

▶

◀

▶

Back

Close

Full Screen / Esc

Printer-friendly Version

Interactive Discussion



The PBL influence at the JFJ as a function of the synoptic weather types is summarized in Fig. 10 which shows the diurnal maxima and minima of the median b_{abs} and N ; the former variable is sensitive to polluted air masses, whereas N is more sensitive to new particle formation and growth. The weather types with advection from W, N and E exhibit the lowest diurnal maximum in b_{abs} and N in winter, involving the smallest PBL influence and lowest concentration of new particles. The PBL influence during the afternoon is shown by diurnal maxima in b_{abs} and occurs from April–September during subsidence (CA) with maxima in July and August. The relatively high diurnal minima in b_{abs} indicate the influence of residual layers at the JFJ during the night for June–August during subsidence (CA) and to a far lesser extent during the CI weather type. All other weather types (CC, M and all advective situations) present higher diurnal maxima in summer but the diurnal minima remain low, leading to a PBL influence during the afternoon but to FT conditions during the night. The growth of newly-formed particles is observed from January–April during lifting (CC) as can be seen in diurnal maxima and minima of N , although this high concentration of new particles can be explained by meteorological parameters and precursor concentrations over the Swiss plateau. Finally, new particle formation is also enhanced during subsidence (CA) due to higher global radiation during the whole year, as can be seen by the higher diurnal maxima in N during the whole year but particularly in September and October.

4.2 Quantification of PBL air masses exported to the JFJ

The export of PBL air masses to the JFJ can be quantified by the relative increase (ri) in the specific humidity and CO concentration (Prévôt et al., 2000; Henne et al., 2004):

$$ri = \frac{C_{\text{JFJ}}(\text{afternoon}) - C_{\text{JFJ}}(\text{morning})}{\text{average}(C_{\text{PAY}}) - C_{\text{JFJ}}(\text{morning})} \quad (1)$$

where C_{JFJ} and C_{PAY} are the concentrations measured at the JFJ and in Payerne, respectively. For the morning and afternoon values, the averaged daily minimum (restricted to the morning between 04:00 and 12:00) and maximum (restricted to the

afternoon between 12:00 and 23:00) were used, respectively. The average in Pay-
erne was taken as the daily average between 09:00 and 20:00. The value of r_i for the
specific humidity was calculated from measurements at Stabio (SwissMetNet station in
Tessin) for AS situations, but r_i for the CO concentration is not reported since CO mea-
surements south of the Alps are only reported for urban areas and are not representa-
tive of the boundary layer concentration. Days with a too high wind velocity (>10 m/s)
and precipitation (>1 mm/day) were excluded from this analysis (Henne et al., 2005b).
When the vertical motion is zero then $r_i=0\%$, whereas a complete replacement of JFJ
by PBL air would yield $r_i=100\%$. The maximum export of PBL air masses occurs during
the CA weather type in the April–August period with respect to specific humidity and
in June–August with respect to CO concentration, reaching 35% and 45%, respec-
tively. For all other weather types, the mean r_i during summer is about 20% for both
the specific humidity and CO concentration. The lowest r_i values (5–10%) are found
in the November–January period for the AW+N+E, CA and CI weather types. Since
the CC weather type is often connected with precipitation, the relative increase in CO
concentration probably leads to a better estimate of the export of PBL air masses to the
JFJ than the specific humidity. The CO relative increase during lifting (CC) is usually
higher than for other weather types, with 25% from April–October, a minimum (7.5%)
in November–January and a maximum in February–March (40%). The M weather type
leads to high r_i for both the specific humidity and CO concentration from February–
May. For the time with the lowest vertical transport (November to January and within
this time period particularly for the weather types AW+N+E), a maximum of 5–10%
of PBL air masses are exported to the JFJ. During strong vertical transport weather
types (CA in April–August, CC in February–March), r_i always remains under 45% so
that the most polluted air masses at the JFJ contain less than 50% of PBL air masses.
In a study concerning two years of reactive nitrogen (NO_y) measurements (Zellweger
et al., 2003), it was concluded that a 14–20% maximum contribution of PBL to FT air
masses occurred during convective weather types, whereas a 12-year analysis of the
specific humidity (Henne et al., 2004) concluded that a maximum of 30% of air masses

**Planetary boundary
influence at the
Jungfrauoch**

M. Collaud Coen et al.

Title Page

Abstract

Introduction

Conclusions

References

Tables

Figures

◀

▶

◀

▶

Back

Close

Full Screen / Esc

Printer-friendly Version

Interactive Discussion



between 2500 and 4000 m a.s.l. originated from the PBL.

5 Conclusions

An analysis of a 14-year dataset (1995–2008) of meteorological and aerosol variables as well as gaseous compounds was performed for different synoptic weather types. Subsidence, lifting and advective weather types present three different seasonalities and lead to various PBL influences at the JFJ. The November–January period is characterized by very low aerosol concentrations and almost no diurnal cycle of the aerosol variables, demonstrating the negligible influence of the PBL for all synoptic weather types except for lifting (CC) which only occurs 6% of the time. In February and March, the lifting weather type makes a large contribution to the aerosol number concentration mainly through the growth of newly formed particles. From March onwards, the subsidence (CA) and convective indifferent (CI) weather types gradually become the dominant weather types, and result in the JFJ being influenced by the PBL during the afternoon, while the night is predominantly influenced by the FT. During summer, the high temperatures lead to PBL influence by thermal convection for all weather types. For subsidence (CA) cases, air masses from residual layers continue to influence the JFJ during the night, leading to higher diurnal minima than for other weather types. Lower W values during CA and generally higher precipitation in August lead to a rapid decrease of the aerosol variables after the temperature maxima at the end of July. A slower decrease is observed in September and October, however, with enhanced new particle formation for the subsidence and CI cases due to higher global radiation with these weather types. The JFJ is negligibly influenced by the PBL during winter for advective weather types. The largest PBL influence is found during summer for the convective anticyclonic weather type, when residual layers influence the JFJ during the night. An analysis of the relative increase of the specific humidity and CO concentration allows us to estimate that on average less than 45% of PBL air is found at the JFJ during all synoptic weather conditions.

Planetary boundary influence at the Jungfraujoch

M. Collaud Coen et al.

Title Page

Abstract

Introduction

Conclusions

References

Tables

Figures

◀

▶

◀

▶

Back

Close

Full Screen / Esc

Printer-friendly Version

Interactive Discussion



Acknowledgements. We thank the International Foundation High Altitude Research Stations Jungfrauoch and Gornergrat (HFSJG), which made it possible to carry out the experiments at the High Altitude Research Station at the Jungfrauoch. We are grateful to the custodians at the Jungfrauoch for their inspection and maintenance of instrumentation. We gratefully
5 acknowledge Ian Colbeck for lending the nephelometer during the first years of measurement at the Jungfrauoch. This work was supported by MeteoSwiss within the Swiss program of the Global Atmosphere Watch (GAW) of the World Meteorological Organization as well as the EU FP6 project EUSAAR. The Swiss National Air Pollution Monitoring Network is run by Empa in joint collaboration with the Swiss Federal Office for the Environment.

10 References

- Anderson, T. L. and Ogren, J. A.: Determining aerosol radiative properties using the TSI 3563 integrating nephelometer, *Aerosol Sci. Technol.*, 29(1), 57–69, 1998.
- Baltensperger, U., Gäggeler, H. W., Jost, D. T., Lugauer, M., Schwikowski, M., Weingartner, E., and Seibert, P.: Aerosol climatology at the high-alpine site Jungfrauoch, Switzerland, *J.*
15 *Geophys. Res.*, 102(D16), 19707–19715, 1997.
- Balzani Lööv, J. M., Henne, S., Legreid, G., Staehelin, J., Reimann, S., Prévôt, A. S. H., Steinbacher, M., and Vollmer, M. K.: Estimation of background concentrations of trace gases at the Swiss Alpine site Jungfrauoch (3580 m a.s.l.), *J. Geophys. Res.*, 113, D22305, doi:10.1029/2007JD009751, 2008.
- 20 Boulon, J., Sellegri, K., Venzac, H., Picard, D., Weingartner, E., Wehrle, G., Collaud Coen, M., Bütikofer, R., Flückiger, E., Baltensperger, U., and Laj, P.: New particle formation and ultrafine charged aerosol climatology at a high altitude site in the Alps (Jungfrauoch, 3580 m a.s.l., Switzerland), *Atmos. Chem. Phys.*, 10, 9333–9349, doi:10.5194/acp-10-9333-2010, 2010.
- 25 Collaud Coen, M., Weingartner, E., Schaub, D., Hueglin, C., Corrigan, C., Henning, S., Schwikowski, M., and Baltensperger, U.: Saharan dust events at the Jungfrauoch: detection by wavelength dependence of the single scattering albedo and first climatology analysis, *Atmos. Chem. Phys.*, 4, 2465–2480, doi:10.5194/acp-4-2465-2004, 2004.
- Collaud Coen, M., Weingartner, E., Nyeki, S., Cozic, J., Henning, S., Verheggen, B., Gehrig, R.,

Planetary boundary influence at the Jungfrauoch

M. Collaud Coen et al.

Title Page

Abstract

Introduction

Conclusions

References

Tables

Figures

◀

▶

◀

▶

Back

Close

Full Screen / Esc

Printer-friendly Version

Interactive Discussion



Planetary boundary influence at the Jungfraujoch

M. Collaud Coen et al.

Title Page

Abstract

Introduction

Conclusions

References

Tables

Figures

◀

▶

◀

▶

Back

Close

Full Screen / Esc

Printer-friendly Version

Interactive Discussion



and Baltensperger, U.: Long-term trend analysis of aerosol variables at the high-alpine site Jungfraujoch, *J. Geophys. Res.*, 112(D13), D13213, 2007.

Collaud Coen, M., Weingartner, E., Apituley, A., Ceburnis, D., Fierz-Schmidhauser, R., Flen-
tje, H., Henzing, J. S., Jennings, S. G., Moerman, M., Petzold, A., Schmid, O., and Bal-
tensperger, U.: Minimizing light absorption measurement artifacts of the Aethalometer: eval-
uation of five correction algorithms, *Atmos. Meas. Tech.*, 3, 457–474, doi:10.5194/amt-3-
457-2010, 2010.

Gibbons, R. D. and Coleman, D. E.: *Statistical Methods for Detection and Quantification of Environmental Contamination*, Wiley-Interscience, New York, USA, 2001.

Henne, S., Furger, M., Nyeki, S., Steinbacher, M., Neininger, B., de Wekker, S. F. J., Dom-
men, J., Spichtinger, N., Stohl, A., and Prévôt, A. S. H.: Quantification of topographic
venting of boundary layer air to the free troposphere, *Atmos. Chem. Phys.*, 4, 497–509,
doi:10.5194/acp-4-497-2004, 2004.

Henne, S., Dommén, J., Neininger, B., Reimann, S., Staehelin, J., and Prévôt, A. S. H.:
Influence of mountain venting in the Alps on the ozone chemistry of the lower
free troposphere and the European pollution export, *J. Geophys. Res.*, 110, D22307,
doi:10.1029/2005JD005936, 2005a.

Henne, S., Furger, M., and Prévôt, A. S. H.: Climatology of mountain venting-induced elevated
moisture layers in the lee of the Alps, *J. Appl. Meteorol.*, 44(5), 620–633, 2005b.

Kammermann, L., Gysel, M., Weingartner, E., and Baltensperger, U.: 13-month climatology of
the aerosol hygroscopicity at the free tropospheric site Jungfraujoch (3580 m a.s.l.), *Atmos.*
Chem. Phys., 10, 10717–10732, doi:10.5194/acp-10-10717-2010, 2010.

Lugauer, M., Baltensperger, U., Furger, M., Gäggeler, H. W., Jost, D. T., Schwikowski, M., and
Wanner, H.: Aerosol transport to the high alpine sites Jungfraujoch (3454 m a.s.l.) and Colle
Gnifetti (4452 m a.s.l.), *Tellus B*, 50(1), 76–92, 1998.

Lugauer, M., Baltensperger, U., Furger, M., Gäggeler, H. W., Jost, D. T., Nyeki, S., and
Schwikowski, M.: Influences of vertical transport and scavenging on aerosol particle sur-
face area and radon decay product concentrations at the Jungfraujoch (3454 m above sea
level), *J. Geophys. Res.*, 105(D15), 19869–19879, 2000.

Manninen, H. E., Nieminen, T., Asmi, E., Gagné, S., Häkkinen, S., Lehtipalo, K., Aalto, P., Vana,
M., Mirme, A., Mirme, S., Hörrak, U., Plass-Dülmer, C., Stange, G., Kiss, G., Hoffer, A., Törö,
N., Moerman, M., Henzing, B., de Leeuw, G., Brinkenberg, M., Kouvarakis, G. N., Bougiatioti,
A., Mihalopoulos, N., O'Dowd, C., Ceburnis, D., Arneth, A., Svenningsson, B., Swietlicki, E.,

Planetary boundary influence at the Jungfraujoch

M. Collaud Coen et al.

Title Page

Abstract

Introduction

Conclusions

References

Tables

Figures

◀

▶

◀

▶

Back

Close

Full Screen / Esc

Printer-friendly Version

Interactive Discussion



Tarozzi, L., Decesari, S., Facchini, M. C., Birmili, W., Sonntag, A., Wiedensohler, A., Boulon, J., Sellegri, K., Laj, P., Gysel, M., Bukowiecki, N., Weingartner, E., Wehrle, G., Laaksonen, A., Hamed, A., Joutsensaari, J., Petäjä, T., Kerminen, V.-M., and Kulmala, M.: EUCAARI ion spectrometer measurements at 12 European sites – analysis of new particle formation events, *Atmos. Chem. Phys.*, 10, 7907–7927, doi:10.5194/acp-10-7907-2010, 2010.

Nessler, R., Weingartner, E., and Baltensperger, U.: Adaptation of dry nephelometer measurements to ambient conditions at the Jungfraujoch, *Environ. Sci. Technol.*, 39(7), 2219–2228, 2005.

Nyeki, S., Baltensperger, U., Colbeck, I., Jost, D. T., Weingartner, E., and Gäggeler, H. W.: The Jungfraujoch high-alpine research station (3454 m) as a background clean continental site for the measurement of aerosol parameters, *J. Geophys. Res.*, 103(D6), 6097–6107, 1998a.

Nyeki, S., Li, F., Weingartner, E., Streit, N., Colbeck, I., Gäggeler, H. W., and Baltensperger, U.: The background aerosol size distribution in the free troposphere: an analysis of the annual cycle at a high-alpine site, *J. Geophys. Res.*, 103(D24), 31749–31761, 1998b.

Nyeki, S., Kalberer, M., Colbeck, I., De Wekker, S., Furger, M., Gäggeler, H. W., Kossmann, M., Lugauer, M., Steyn, D., Weingartner, E., Wirth, M., and Baltensperger, U.: Convective boundary layer evolution to 4 km a.s.l. over high-alpine terrain: airborne lidar observations in the Alps, *Geophys. Res. Lett.*, 27(5), 689–692, 2000.

Prévôt, A. S. H., Dommen, J., and Bäumle, M.: Influence of road traffic on volatile organic compound concentrations in and above a deep alpine valley, *Atmos. Environ.*, 34(27), 4719–4726, 2000.

Schüepp, M.: Witterungsklimatologie, *Klimatologie der Schweiz*, Band III, Beilage zu den Annalen 1978, MeteoSwiss, Zürich, Switzerland, 1979.

Schüepp, M. and Schirmer, H.: Climates of central Europe, in *Climates of Central and Southern Europe*, *World Survey of Climatology*, 6, 3–73, 1977.

Schwarb, M.: Witterungsanalyse anhand der Alpenwetterstatistik mit Bezug auf den Niederschlag, Period 1945–1994, *Berichte und Skripten Geogr. Institut ETH Zürich* 58, Zürich, 1996.

SMI (Swiss Meteorological Institut): *Alpenwetterstatistik Witterungskalender*, Beschreibung der einzelnen Parameter, MeteoSwiss, Zürich, 1985.

Stefanicki, G., Talkner, P., and Weber, R. O.: Frequency changes of weather types in the alpine region since 1945, *Theor. Appl. Climatol.*, 60(1), 47–61, 1998.

Urfer, C.: Die Klimaregionen der Schweiz: *Alpenordhang*, *Klimatologie der Schweiz*, 2, 2–247,

1979.

Wanner, H., Salvisberg, E., Rickli, R., and Schüepp, M.: 50 years of Alpine Weather Statistics (AWS), *Meteorol. Z.*, 7(3), 99–111, 1998.

Weingartner, E., Nyeki, S., and Baltensperger, U.: Seasonal and diurnal variation of aerosol size distributions ($10 < D < 750$ nm) at a high-alpine site (Jungfrauoch 3580 m a.s.l.), *J. Geophys. Res.*, 104(D21), 26809–26820, 1999.

Weingartner, E., Saathoff, H., Schnaiter, M., Streit, N., Bitnar, B., and Baltensperger, U.: Absorption of light by soot particles: determination of the absorption coefficient by means of aethalometers, *J. Aerosol Sci.*, 34(10), 1445–1463, 2003.

Zellweger, C., Ammann, M., Buchmann, B., Hofer, P., Lugauer, M., Rüttimann, R., Streit, N., Weingartner, E., and Baltensperger, U.: Summertime NO_y specification at the Jungfrauoch, 3580 m a.s.l., Switzerland, *J. Geophys. Res.*, 105, 6655–6667, 2000.

Zellweger, C., Forrer, J., Hofer, P., Nyeki, S., Schwarzenbach, B., Weingartner, E., Ammann, M., and Baltensperger, U.: Partitioning of reactive nitrogen (NO_y) and dependence on meteorological conditions in the lower free troposphere, *Atmos. Chem. Phys.*, 3, 779–796, doi:10.5194/acp-3-779-2003, 2003.

ACPD

11, 985–1024, 2011

Planetary boundary influence at the Jungfrauoch

M. Collaud Coen et al.

Title Page

Abstract

Introduction

Conclusions

References

Tables

Figures

◀

▶

◀

▶

Back

Close

Full Screen / Esc

Printer-friendly Version

Interactive Discussion



Planetary boundary influence at the Jungfraujoch

M. Collaud Coen et al.

Table 1. The synoptic weather types of the alpine weather statistics scheme, described by 3 basic types, 8 extended types, and by the dominant synoptic scale motion.

Basic weather type	Extended types	Abbreviation	Synoptic motion
Convective	Anticyclonic	CA	Subsidence
	Indifferent	CI	Small-scale circulations
	Cyclonic	CC	Lifting
Advective	West	AW	W at 500 hPa
	North	AN	NW-N at 500 hPa
	East	AE	NE-SE at 500 hPa
	South	AS	S-SW at 500 hPa
Mixed		M	Active cyclone or jet flow

Title Page

Abstract

Introduction

Conclusions

References

Tables

Figures

◀

▶

◀

▶

Back

Close

Full Screen / Esc

Printer-friendly Version

Interactive Discussion



Planetary boundary influence at the Jungfraujoch

M. Collaud Coen et al.

Table 2. Yearly frequency distribution in percent of weather types for 1945–1994 (Wanner et al., 1998), 1988–1996 (Lugauer et al., 1998) and 1995–2008. For the 1995–2008 period (this work) the spread in data corresponding to two standard deviations is given.

	CA	CI	CC	A	M
1945–1994	16.5	27.4	7.4	42.6	6.2
1988–1996	23.0	31.3	6.4	35.4	3.9
1995–2008	20.9±9.2	30.3±8.0	6.7±4.6	35.7±6.0	6.4±3.8

[Title Page](#)
[Abstract](#)
[Introduction](#)
[Conclusions](#)
[References](#)
[Tables](#)
[Figures](#)
[Back](#)
[Close](#)
[Full Screen / Esc](#)
[Printer-friendly Version](#)
[Interactive Discussion](#)


Planetary boundary influence at the Jungfraujoch

M. Collaud Coen et al.

Table 3. Diurnal cycle amplitude (maximum/minimum) for the temperature and the relative humidity as a function of the season and the synoptic weather type.

WL Season	T_{\max}/T_{\min}					RH_{\max}/RH_{\min}				
	Nov–Jan	Feb–Mar	Apr–May	Jun–Aug	Sep–Oct	Nov–Jan	Feb–Mar	Apr–May	Jun–Aug	Sep–Oct
CA	1.10	1.13	1.26	1.47	1.26	1.06	1.11	1.42	1.36	1.21
CI	1.06	1.09	1.19	1.28	1.16	1.03	1.09	1.16	1.22	1.14
CC	1.06	1.05	1.11	1.16	1.09	1.08	1.12	1.11	1.14	1.09
AW+N+E	1.08	1.09	1.14	1.27	1.14	1.16	1.30	1.11	1.15	1.16
AS	1.06	1.04	1.13	1.19	1.08	1.12	1.13	1.13	1.45	1.10
M	1.03	1.04	1.09	1.11	1.07	1.08	1.06	1.15	1.23	1.11

Title Page

Abstract

Introduction

Conclusions

References

Tables

Figures

⏪

⏩

◀

▶

Back

Close

Full Screen / Esc

Printer-friendly Version

Interactive Discussion



Planetary boundary influence at the Jungfraujoch

M. Collaud Coen et al.

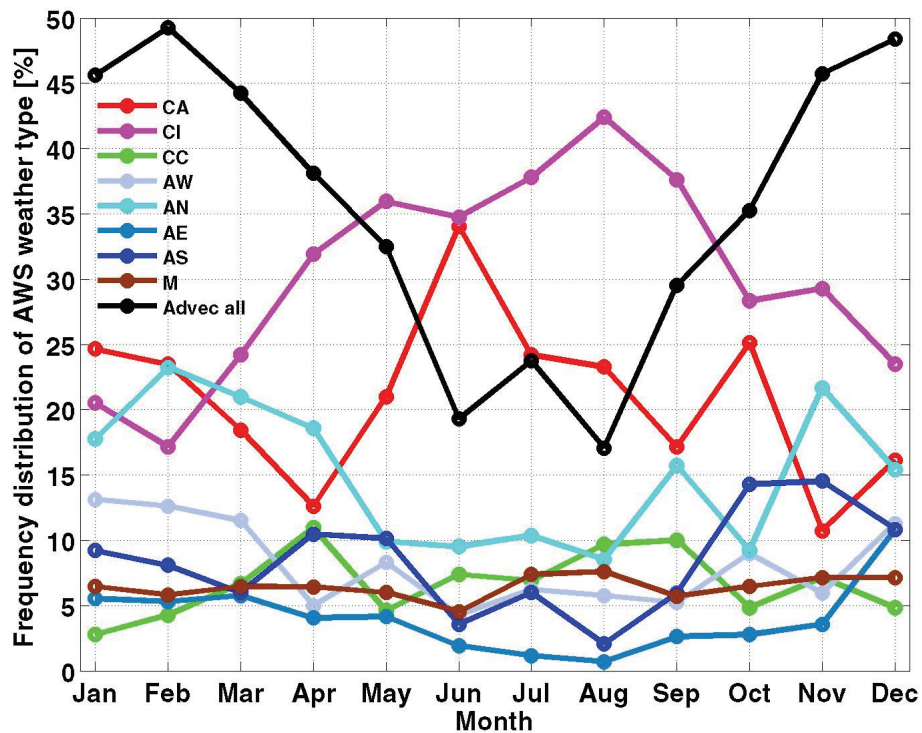


Fig. 1. Monthly frequency distribution of AWS weather types for the 1995–2008 period.

Title Page

Abstract

Introduction

Conclusions

References

Tables

Figures

◀

▶

◀

▶

Back

Close

Full Screen / Esc

Printer-friendly Version

Interactive Discussion



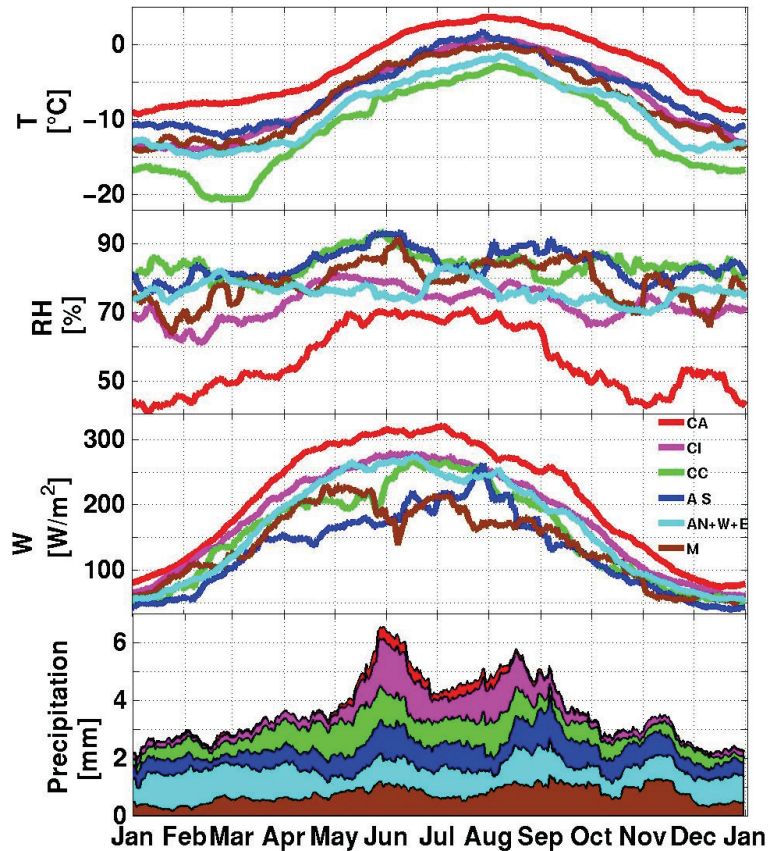


Fig. 2. Mean 1995–2008 annual cycles of the temperature T , the RH, the global short wave radiation W at the JFJ and the precipitation at the Kleine Scheidegg as a function of AWS weather types.

Planetary boundary influence at the Jungfraujoch

M. Collaud Coen et al.

Title Page

Abstract Introduction

Conclusions References

Tables Figures

◀ ▶

◀ ▶

Back Close

Full Screen / Esc

Printer-friendly Version

Interactive Discussion



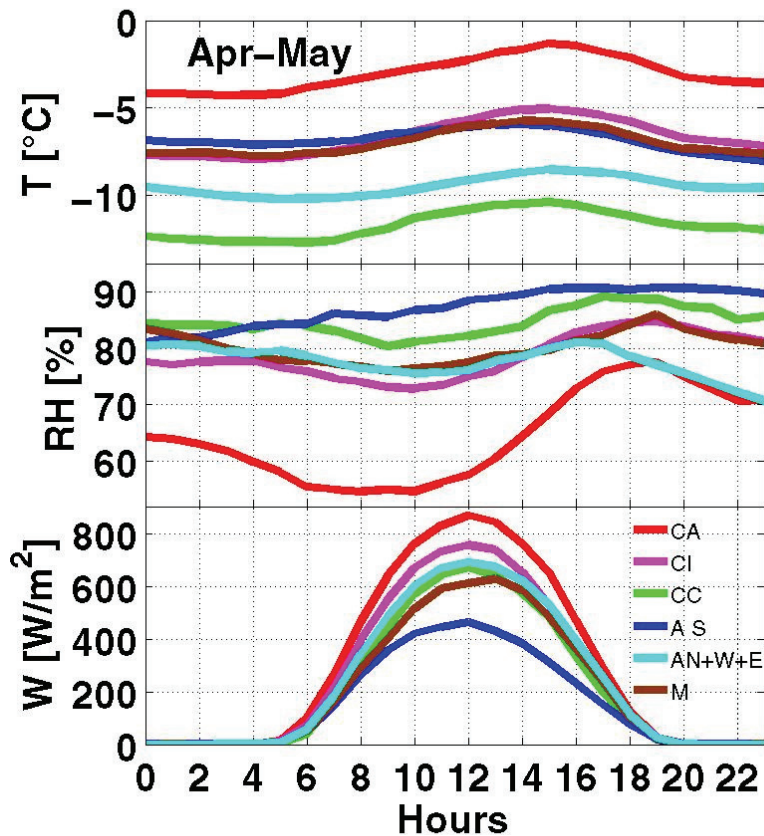


Fig. 3. Mean 1995–2008 diurnal cycles of the temperature, the relative humidity percentage RH and the global short wave radiation W for the April-May period as a function of AWS weather types.

Planetary boundary influence at the Jungfrauoch

M. Collaud Coen et al.

Title Page

Abstract Introduction

Conclusions References

Tables Figures

◀ ▶

◀ ▶

Back Close

Full Screen / Esc

Printer-friendly Version

Interactive Discussion



Planetary boundary influence at the Jungfraujoch

M. Collaud Coen et al.

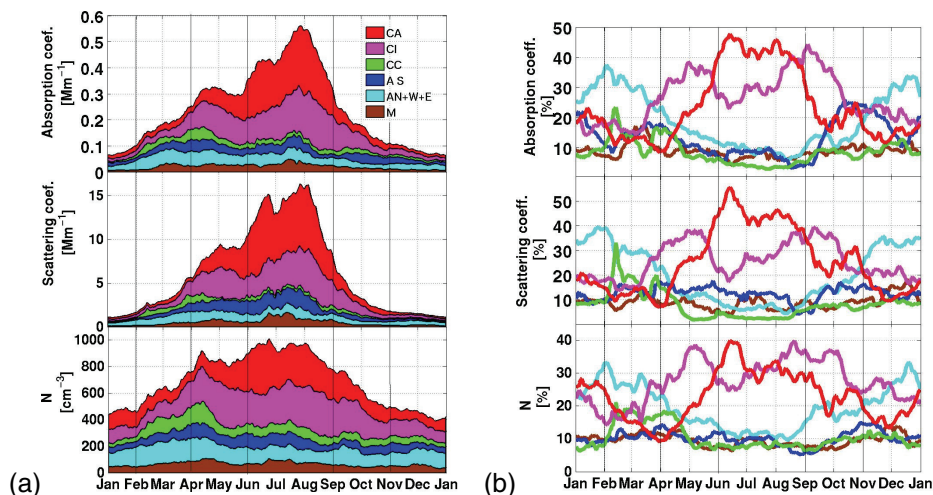


Fig. 4. Median 1995–2008 annual cycles of the absorption coefficient at $\lambda=880$ nm, the scattering coefficient at $\lambda=550$ nm and the aerosol number concentration as a function of AWS weather types: **(a)** summed contributions of each weather type as a function of the measured variables during each weather type and its frequency of occurrence, **(b)** relative contributions of each weather type in %.

Title Page

Abstract

Introduction

Conclusions

References

Tables

Figures

◀

▶

◀

▶

Back

Close

Full Screen / Esc

Printer-friendly Version

Interactive Discussion



Planetary boundary influence at the Jungfraujoch

M. Collaud Coen et al.

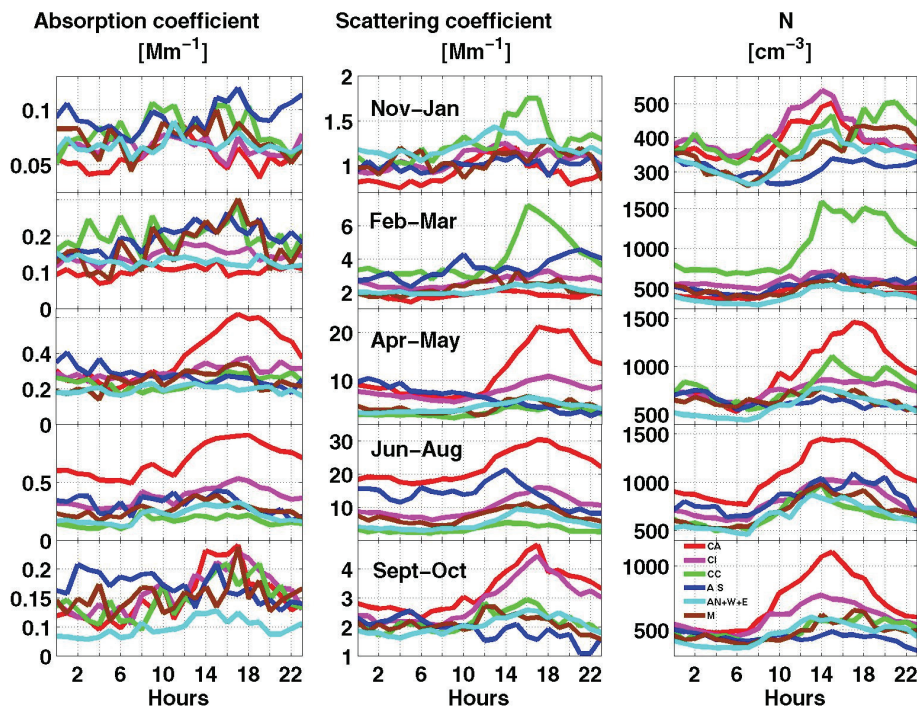


Fig. 5. Median 1995–2008 diurnal cycles of the absorption coefficient at $\lambda=880$ nm, the scattering coefficient at $\lambda=550$ nm and the aerosol number concentration for 5 defined periods of the year (see middle graph for definition) as a function of AWS weather types.

[Title Page](#)
[Abstract](#)
[Introduction](#)
[Conclusions](#)
[References](#)
[Tables](#)
[Figures](#)
[◀](#)
[▶](#)
[◀](#)
[▶](#)
[Back](#)
[Close](#)
[Full Screen / Esc](#)
[Printer-friendly Version](#)
[Interactive Discussion](#)


Planetary boundary influence at the Jungfraujoch

M. Collaud Coen et al.

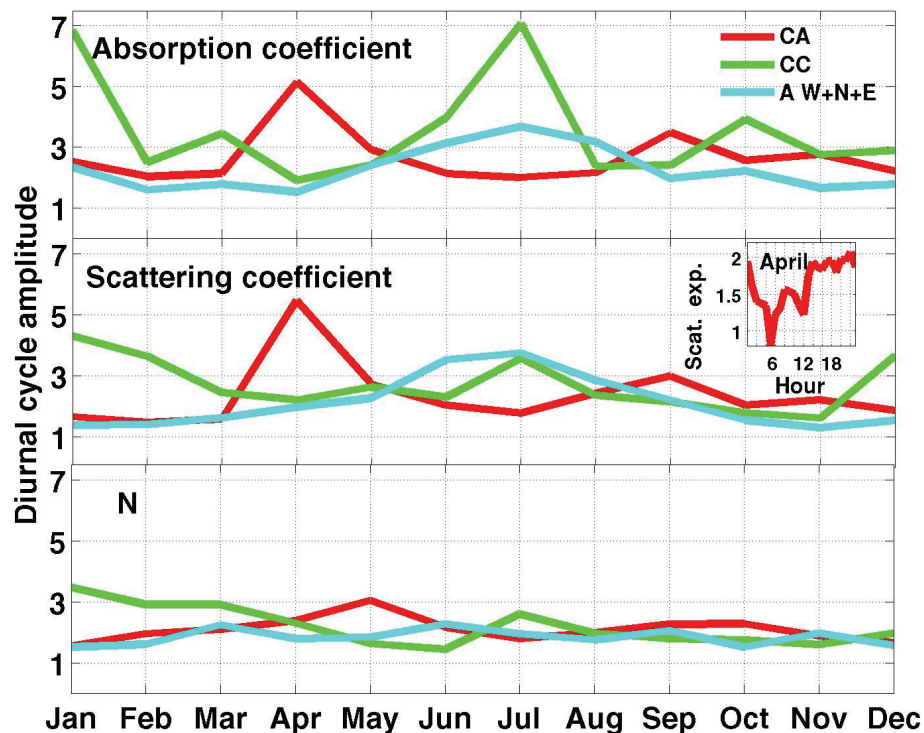


Fig. 6. Amplitude (max/min) of the diurnal cycles of b_{abs} , b_{scat} and N concentration for CA (subsidence), CC (lifting) and advective weather types from W, N and E. Inset shows the April diurnal cycle of the scattering Ångström exponent at 550 nm.

Title Page

Abstract

Introduction

Conclusions

References

Tables

Figures

◀

▶

◀

▶

Back

Close

Full Screen / Esc

Printer-friendly Version

Interactive Discussion



**Planetary boundary
influence at the
Jungfraujoch**

M. Collaud Coen et al.

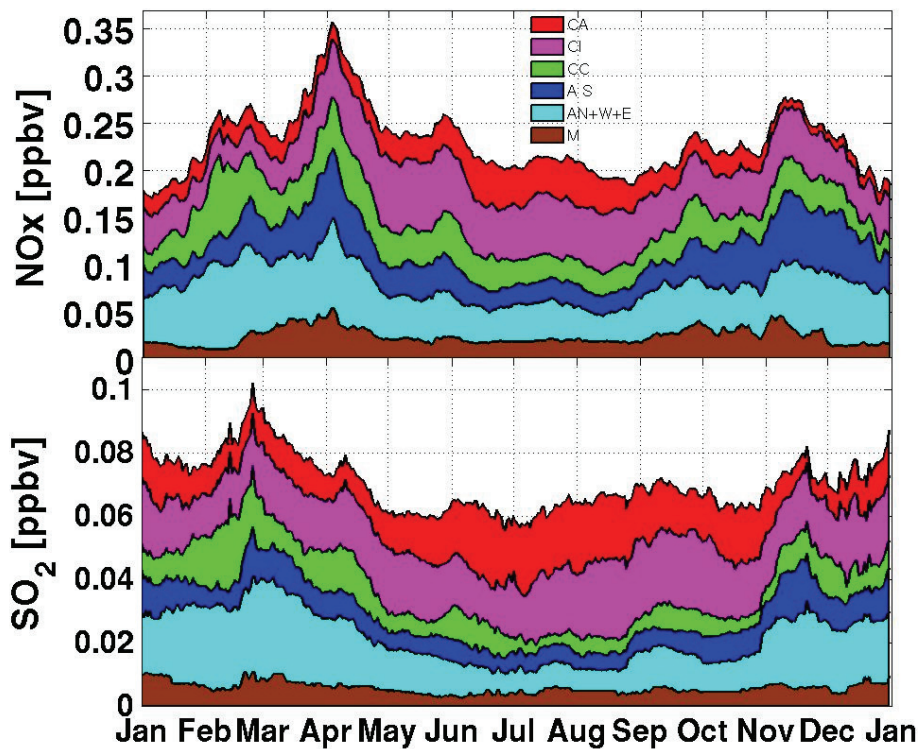


Fig. 7. Mean 1995–2008 annual cycles of NO_x and SO₂ concentrations as a function of AWS weather types.

[Title Page](#)[Abstract](#)[Introduction](#)[Conclusions](#)[References](#)[Tables](#)[Figures](#)[◀](#)[▶](#)[◀](#)[▶](#)[Back](#)[Close](#)[Full Screen / Esc](#)[Printer-friendly Version](#)[Interactive Discussion](#)

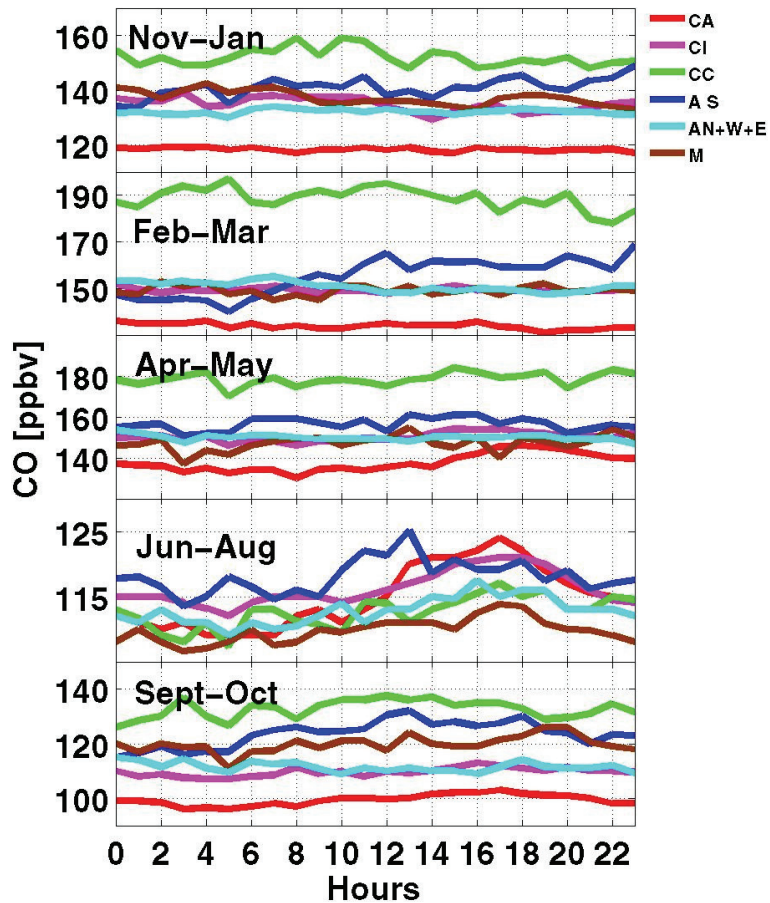


Fig. 8. Median 1995–2008 diurnal cycles of CO concentration for the 5 defined periods of the year as a function of AWS weather types.

Planetary boundary influence at the Jungfraujoch

M. Collaud Coen et al.

Title Page

Abstract Introduction

Conclusions References

Tables Figures

◀ ▶

◀ ▶

Back Close

Full Screen / Esc

Printer-friendly Version

Interactive Discussion



Planetary boundary influence at the Jungfraujoch

M. Collaud Coen et al.

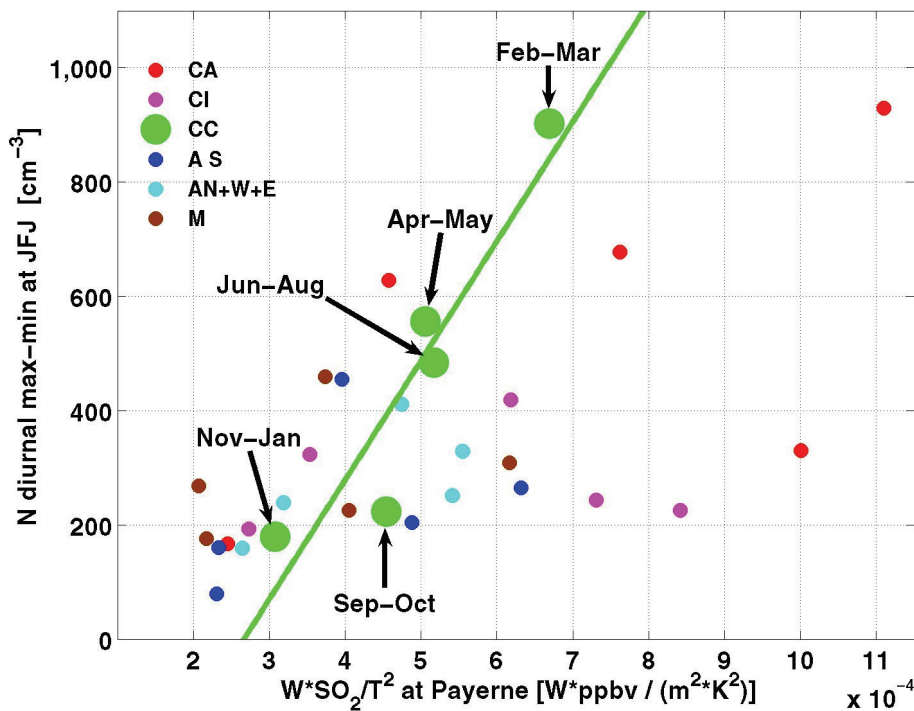


Fig. 9. Difference between the diurnal maximum and minimum in median N values measured at the JFJ versus $W \cdot \text{SO}_2 / T^2$ measured at Payerne (Swiss plateau) for different AWS weather types and periods of the year.

Title Page

Abstract

Introduction

Conclusions

References

Tables

Figures

◀

▶

◀

▶

Back

Close

Full Screen / Esc

Printer-friendly Version

Interactive Discussion



Planetary boundary influence at the Jungfraujoch

M. Collaud Coen et al.

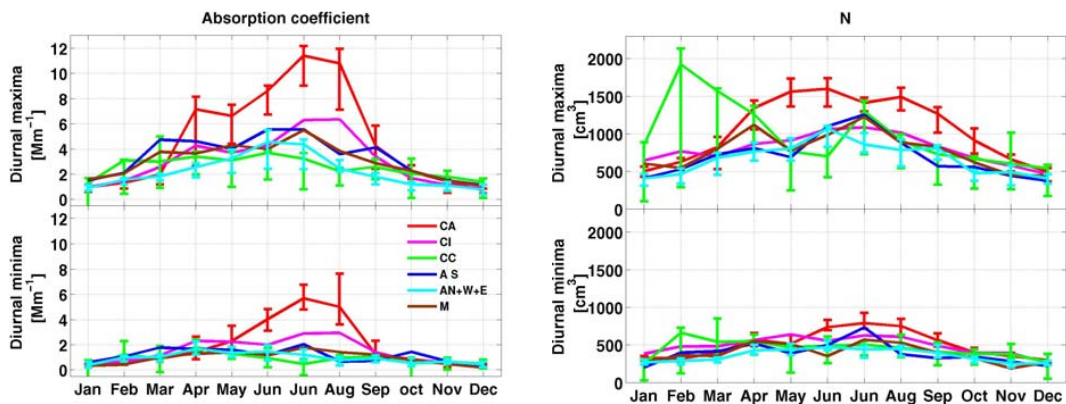


Fig. 10. Monthly diurnal maxima and minima of b_{abs} and N as a function of AWS weather types.

Title Page

Abstract

Introduction

Conclusions

References

Tables

Figures

◀

▶

◀

▶

Back

Close

Full Screen / Esc

Printer-friendly Version

Interactive Discussion



Planetary boundary influence at the Jungfraujoch

M. Collaud Coen et al.

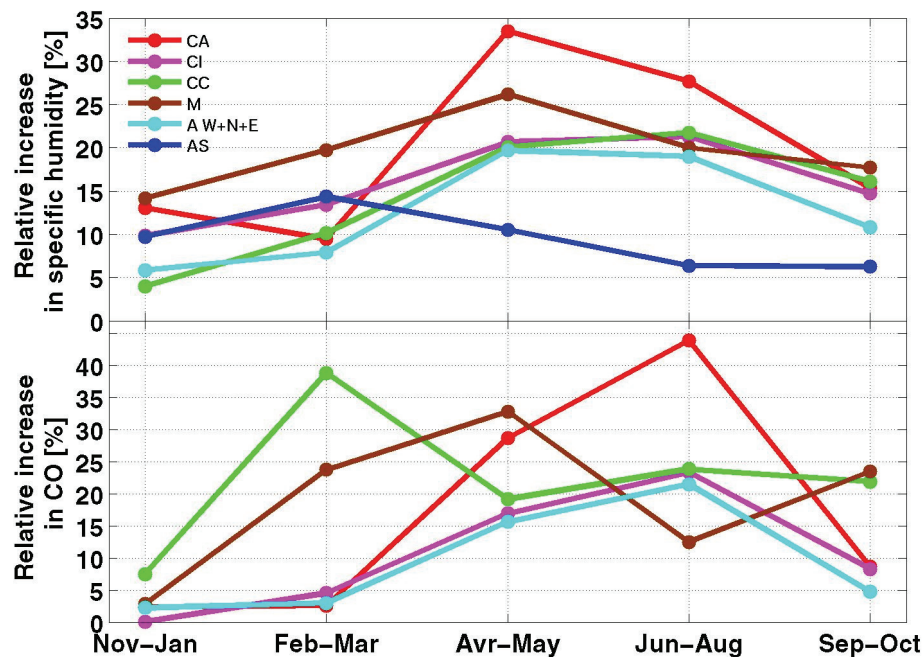


Fig. 11. Relative increase in the specific humidity and in CO concentration calculated from JFJ and Payerne data for all weather types and for the defined periods of the year. Data for the AS weather type was taken from the Stabio site, south of the Alps.

Title Page

Abstract

Introduction

Conclusions

References

Tables

Figures

◀

▶

◀

▶

Back

Close

Full Screen / Esc

Printer-friendly Version

Interactive Discussion

